Scientific Contributions Oil & Gas, Vol. 49. No. 2, June: 409 - 430

SCIENTIFIC CONTRIBUTIONS OIL AND GAS

Testing Center for Oil and Gas
LEMIGAS

Journal Homepage:http://journal.lemigas.esdm.go.id
ISSN: 2089-3361, e-ISSN: 2541-0520

Optimization of Chemicaly Activated Candlenut and Walnut Shell Biosorbents for Produced Water Purification Within an IoT-Based Monitoring System

Muhammad Khairul Afdhol[1,2], Rika Lala Saputri[1], Mursyidah[1], Fiki Hidayat[1], Tomi Erfando[1], Ari Prasetyo[3], and Adiella Zakky Juneid[4]

[1]Department of Petroleum Engineering, Faculty of Engineering, Universitas Islam Riau
Kaharuddin Nasution Street No. 113, Simpang Tiga, Pekanbaru, Indonesia

[2]Departement of Research and Study PT. Durazid Vidya Daksa,
Sisingamangaraja Street No. 45A Bangkinang, Kampar, Indonesia.

[3]Department of Mechanical Engineering, Faculty of Engineering, Universitas Islam Riau
Kaharuddin Nasution Street No. 113, Simpang Tiga, Pekanbaru, Indonesia

[4]Physics Education, Faculty of Teacher and Education, Universitas Riau,
Kampus Bina Widya KM. 12,5, Simpang Baru, Kec. Tampan, Pekanbaru, Indonesia.

Corresponding author: Muhammad Khairul Afdhol (afdhol@eng.uir.ac.id)

Manuscript received: February 27th, 2026; Revised: April 01st, 2026
Approved: May 04th, 2026; Available online: June 15th, 2026; Published: June 15th, 2026.

ABSTRACT - Produced water from petroleum operations contains high levels of hydrocarbons, suspended solids, and dissolved contaminants that must be treated before discharge or reuse. This study aims to optimize biosorbents derived from candlenut and walnut shells through chemical activation using potassium hydroxide (KOH) for the purification of produced water. In addition, an Internet of Things (IoT)-based monitoring system is integrated to enable real-time assessment of water quality parameters. The biosorbents are characterized using Fourier Transform Infrared Spectroscopy (FTIR) and Scanning Electron Microscopy (SEM) to identify surface functional groups and morphological modifications. Experimental evaluations of turbidity, bulk density, and total dissolved solids (TDS) are conducted under various operating conditions. The activated biosorbents exhibited enhanced hydroxyl and carboxyl functional groups, as confirmed by FTIR, with an optimal bulk density of 0.76 g/cm³. Under optimum conditions (pH 7, contact time 90 min, adsorbent dosage 15 g/L), turbidity and TDS removals reached 80% and 75%, respectively. The IoT system successfully enabled real-time data acquisition and process monitoring, ensuring operational reliability. The maximum adsorption capacity based on the Langmuir model reached 33.8 mg/g for KOH-activated walnut and 31.2 mg/g for candlenut biosorbent. Overall, the chemically activated candlenut and walnut biosorbents demonstrated excellent adsorption capacity and potential for sustainable produced water treatment. This approach offers an environmentally friendly and cost-effective solution by utilizing local biomass waste integrated with modern IoT-based control technologies. Adsorption behavior is further evaluated using Langmuir/Freundlich isotherm and kinetic models.

Keywords: Biosorption, produced water, chemical activation, walnut shell, IoT monitoring, sustainable water treatment

How to cite this article:

Muhammad Khairul Afdhol, Rika Lala Saputri, Mursyidah, Fiki Hidayat, Tomi Erfando, Ari Prasetyo, and Adiella Zakky Juneid, 2026, Optimization of Chemicaly Activated Candlenut and Walnut Shell Biosorbents for Produced Water Purification Within an IoT-Based Monitoring System, Scientific Contributions Oil and Gas, 49 (2) pp. 409 - 430. DOI org/10.29017/scog.v49i2.1972.

INTRODUCTION

The global oil and gas industry generates approximately 250 million barrels of produced water every day, making it the largest waste stream associated with petroleum operations (Ibrahim et al., 2023. Produced water contains a complex mixture of hydrocarbons, suspended solids, dissolved salts, and residual production chemicals that require advanced treatment before being discharged or reused (Liu et al., 2021). Conventional treatment technologies such as chemical coagulation, membrane filtration, and electrochemical processes often suffer from high operational costs, complex maintenance requirements, and secondary pollution issues (Koul et al., 2022; Gangwar et al., 2025). Therefore, the present study extends previous work by comparing candlenut and walnut biosorbents, applying comprehensive adsorption modeling, and improving IoT-based monitoring validation for sustainable produced water treatment.Therefore, there is an urgent need for low-cost and sustainable alternatives to mitigate the environmental impacts of produced water disposal.

Various biomass materials such as coconut shell, palm kernel shell, rice husk, sawdust, bamboo root and corn cob have previously been investigated as biosorbents for wastewater treatment due to their low cost and abundant availability (Wulandari et al., 2023). However, several limitations remain, including low adsorption selectivity, limited mechanical stability, poor pore uniformity, and reduced adsorption efficiency under high-salinity produced water conditions. Compared with these materials, candlenut and walnut shells possess higher lignin and fixed-carbon contents, stronger structural stability, and greater potential for chemical activation, making them promising candidates for produced water purification applications.

Previous research by Afdhol et al. (2025) investigated zinc chloride-activated candlenut adsorbent integrated with IoT monitoring for produced water filtration. Although the study demonstrated promising filtration performance, several limitations were identified. The previous work only focused on a single biomass source, lacked comparative evaluation with other biosorbents, and did not include comprehensive adsorption isotherm, kinetic, and thermodynamic analyses. In addition, the IoT system was primarily utilized for basic monitoring without detailed validation of sensor reliability and real-time analytical performance. Therefore, further investigation is required to improve both adsorption performance evaluation and IoT-based monitoring integration.

Adsorption using solid sorbents is widely recognized as one of the most efficient and cost-effective techniques for removing contaminants from industrial effluents. However, traditional adsorbents—typically derived from fossil-based materials—lack sustainability and may contribute to secondary contamination. In recent years, biosorbents derived from lignocellulosic biomass have gained increasing attention as eco-friendly and renewable alternatives due to their high surface area, porosity, and abundance of reactive functional groups (Osman et al., 2023. The valorization of agricultural and forestry residues into biosorbents aligns with circular economy principles, providing a dual benefit of waste minimization and water remediation (Omran & Baek 2022).

Among various biomass sources, candlenut (Aleurites moluccanus) and walnut (Juglans regia) shells have shown promising potential owing to their high lignin and cellulose contents, mechanical strength, and porous structure. Previous studies demonstrated the ability of walnut shells to adsorb radionuclides and organic pollutants effectively (Al-Masri et al., 2021; Enache et al., 2023). Nevertheless, most reported works focus on single-contaminant systems or simple physical modifications. Systematic investigations on chemical activation strategies specifically tailored for the complex matrix of produced water remain limited. Chemical activation, particularly using alkaline agents such as potassium hydroxide (KOH), can significantly enhance pore formation and surface reactivity by promoting dehydration and gasification reactions (Leng et al., 2021).

Furthermore, recent advancements in the Internet of Things (IoT) have enabled real-time monitoring and intelligent control of water treatment processes. IoT-based sensor networks allow continuous tracking of important water quality parameters such as turbidity, TDS, pH, and temperature, thereby improving operational efficiency, predictive maintenance, and decision-making accuracy (Alshami et al., 2024; Forhad et al., 2024). The implementation of IoT is particularly beneficial for remote oilfield operations where continuous manual monitoring is difficult to perform.

Adsorption isotherm and kinetic modeling are important approaches for understanding adsorption mechanisms, adsorption capacity, and rate-controlling processes in produced water treatment systems. Therefore, this study aims to optimize the chemical activation of candlenut and walnut shell biosorbents using potassium hydroxide for the purification of produced water from oilfield operations. Additionally, an IoT-based monitoring system was developed to provide real-time data acquisition and control of filtration parameters. The outcomes of this research are expected to contribute to the development of a sustainable, low-cost, and digitally integrated biosorption technology for produced water management in the upstream petroleum industry. This study is the first to integrate chemical–activated local biomass (candlenut and walnut shells) into a real-time IoT monitoring system for produced-water purification.

MATERIAL AND METHOD

This study evaluated the performance of chemically activated candlenut and walnut shell biosorbents for produced water treatment under various operational conditions. The investigated parameters included solution pH (5–9), contact time (30–120 min), adsorbent dosage (5–20 g/L), and operating temperature (40–60°C). The measured responses consisted of turbidity removal, total dissolved solids (TDS) reduction, adsorption capacity (mg/g), bulk density, and biosorbent surface characteristics analyzed using FTIR and SEM. In addition, the reliability of the IoT-based monitoring system was evaluated through comparison with laboratory measurements.

Preparation of biosorbents

Candlenut (Aleurites moluccanus) and walnut (Juglans regia) shells were collected from local agricultural residues in Riau Province, Indonesia. The shells were washed thoroughly with deionized water to remove impurities, oven-dried at 105 °C for 24 hours, and then crushed and sieved using a 16-mesh (1.18 mm) sieve to obtain uniform particle size distribution. The cleaned and sieved materials were stored in airtight containers prior to chemical activation (Afdhol, Saputri, et al., 2025; Saputri et al., 2025).

Chemical activation process

The dried biomass samples were chemically activated using a potassium hydroxide (KOH) solution to enhance surface porosity and develop active functional groups. The impregnation process was conducted in a 1 L glass reactor equipped with a mechanical stirrer. The biomass-to-activating agent ratio was maintained at 1:3 (w/w), and the mixture was stirred continuously at 300 rpm for 2 hours at 80 °C. After activation, the materials were repeatedly washed with deionized water until the filtrate reached a neutral pH (≈7). The neutralized biosorbents were oven-dried again at 105°C for 12 hours and stored in desiccators until further characterization (Leng et al., 2021; Afdhol, Juneid, et al., 2025).

Characterization of biosorbents

Bulk density measurement

Bulk density was determined using a Tapped Density Meter (Model MM-0101). Approximately 100 mL of the dried biosorbent was transferred into a graduated cylinder without compaction. The cylinder was tapped 500 and 1200 times sequentially, and the bulk density (ρ_bulk) was calculated using Equation 1

$$\rho_{bulk} = \frac{m}{V_{bulk}} \qquad (1)$$

where m is the mass of the sample (g) and V_bulk is the final tapped volume (mL). Each test was performed in triplicate to ensure statistical reliability (Campiñez et al., 2016).

Fourier transform infrared spectroscopy (FTIR)

FTIR analysis was conducted using a Shimadzu IR Prestige-21 spectrophotometer to identify the functional groups present on the biosorbent surface before and after chemical activation. Prior to analysis, the dried biosorbent samples were finely ground and mixed with KBr powder to form pellets. Spectra were recorded within the wavenumber range of 4000–400 cm^{-1} (Wulandari et al., 2022. The obtained spectra were analyzed to identify hydroxyl (–OH), carbonyl (C=O), and ether (C–O–C) functional groups associated with lignocellulosic structures (Guerrero-Pérez & Patience 2020; Mukai et al., 2021).

Scanning electron microscopy (SEM)

Surface morphology and pore structure of the biosorbents were analyzed using a JEOL JSM-6460LA Scanning Electron Microscope operated at an accelerating voltage of 15 kV. Before imaging, the samples were oven-dried and coated with a thin gold layer using a sputter coater to improve electrical conductivity and image clarity (Wulandari et al., 2024. SEM observations were performed at various magnifications to evaluate pore development, surface roughness, and structural changes induced by KOH activation (Arora et al., 2020).

Filtration and water quality analysis

Turbidity measurement

Filtration experiments were conducted using produced water obtained from an oilfield in Riau Province. The produced water exhibited an initial turbidity of 450–500 NTU. The filtrate turbidity was measured using an IoT-integrated turbidity sensor system that continuously monitored both inlet and outlet streams. Temperature conditions were maintained at 40 °C and 60 °C to investigate the effect of thermal variation on adsorption efficiency. The IoT platform automatically recorded data at 1-minute intervals and transmitted it via a wireless module for real-time visualization and analysis (Pasika & Gandla 2020).

Total dissolved solids (TDS) measurement

TDS concentration was measured using a calibrated IoT-based TDS sensor integrated into the same monitoring system. The sensors operated based on electrical conductivity measurements, with data transmitted to a central microcontroller (ESP32) and displayed through a web-based dashboard. The system allowed continuous observation of TDS removal trends and predictive maintenance scheduling (Sulistiyanto et al., 2023; Forhad et al., 2024).

Performance Evaluation:

Turbidity and TDS removal efficiencies (ç) were calculated using Equation 2

$$\eta = \frac{C_i - C_f}{C_i} \times 100\% \qquad (2)$$

where Ci and Cf are the initial and final concentrations, respectively.

Experimental design and optimization

Batch adsorption experiments were performed under varying pH (5–9), contact time (30–120 min), and adsorbent dosage (5–20 g L^{-1}) to determine optimal operating conditions. All experiments were conducted in triplicate, and average values were reported. The effect of temperature on adsorption efficiency was also analyzed to simulate field-relevant thermal conditions. In addition, the treatment system configuration used in this study is illustrated in Figure 1. The diagram presents the integration of IoT technology into the produced water treatment

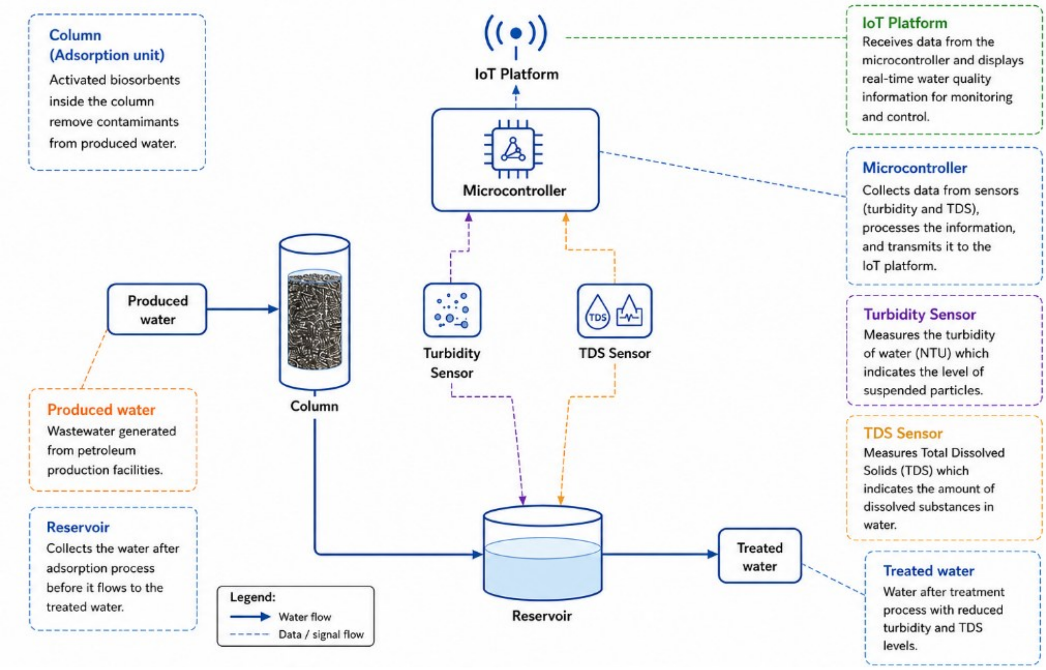

Figure 1. Schematic diagram of the IoT-based produced water treatment system. Produced water is treated in an adsorption column before being discharged as treated water. Turbidity and TDS sensors provide continuous measurements of water quality, and the acquired data are processed by a microcontroller and transmitted to the IoT platform for real-time monitoring and operational decision-making.

Table 1. IoT-Integrated flow diagram of produced water treatment setup

Parameter	Symbol / Unit	Type of variable	Range / Level	Purpose / Description
Adsorbent type	–	Independent	Candlenut (KMR), Walnut (WN)	To compare performance of two biosorbents derived from local biomass.
Chemical activation agent	–	Independent	KOH (1.0 M)	To enhance porosity and surface functional groups.
Impregnation ratio (biomass: KOH)	–	Controlled	1:3 (w/w)	Standardized for consistent surface activation.
Activation temperature	°C	Controlled	80 °C	Promotes pore formation and functionalization.
Drying temperature	°C	Controlled	105 °C	Ensures moisture removal before and after activation.
Solution pH	pH	Independent	5, 7, 9	To determine pH effect on adsorption efficiency.
Contact time	t (min)	Independent	30, 60, 90, 120	Evaluates adsorption kinetics and equilibrium time.
Adsorbent dosage	D ($g \cdot L^{-1}$)	Independent	5, 10, 15, 20	To identify optimum adsorbent mass for removal performance.
Temperature	T (°C)	Independent	40, 60	Simulates field thermal variation in produced water.
Mixing speed	rpm	Controlled	300	Ensures homogenous contact between adsorbent and solution.
Produced water source	–	Fixed	Oilfield in Riau Province, Indonesia	Representative sample of industrial produced water.
Measured responses	–	Dependent	Turbidity (NTU), TDS (ppm), Bulk density (g/cm^3)	Key output parameters for evaluating purification efficiency.
Monitoring system	–	Fixed	IoT-based (ESP32, turbidity & TDS sensors)	Enables real-time monitoring and data acquisition.
Replication	–	Controlled	n = 3 (triplicate)	Ensures statistical reliability of results.

process through real-time monitoring using turbidity and TDS sensors connected to a microcontroller and IoT platform to enhance treatment efficiency and operational monitoring.

Table 1 summarizes the experimental variables and operating parameters applied in the IoT-integrated produced water treatment system. The table includes the independent, controlled, and dependent variables used to evaluate the adsorption performance of candlenut and walnut shell biosorbents under different operational conditions. The prepared biosorbents and IoT-integrated filtration system were subsequently evaluated to determine their physicochemical characteristics, adsorption performance, and real-time monitoring capability under various operating conditions.

RESULT AND DISCUSSION

The IoT-based monitoring system implemented in this study utilized an Arduino Uno R3 microcontroller board as the main data acquisition and processing unit, as illustrated in Figure 2. The microcontroller was integrated with turbidity, TDS, temperature, and pH sensors to enable real-time monitoring and transmission of produced water quality data during the adsorption process.

Bulk density analysis

Figure 3 shows the bulk density of candlenut and walnut biosorbents before and after KOH activation. The candlenut biosorbent exhibited a slightly higher bulk density (0.76 g/cm³) compared to walnut (0.71 g/cm³), which is attributed to its denser lignocellulosic matrix and higher lignin content. After KOH activation, both materials showed a moderate reduction in bulk density, with an average decrease of 1.3%. This reduction is consistent with the formation of micro- and mesopores during the alkaline activation process, where dehydration and partial gasification reactions occur between KOH and organic components (Leng et al., 2021).

Mathematically, the change in bulk density (Δρ) can be expressed as shown in Equation 3,

$$\Delta\rho = \rho_{\text{initial}} - \rho_{\text{activated}} \quad (3)$$

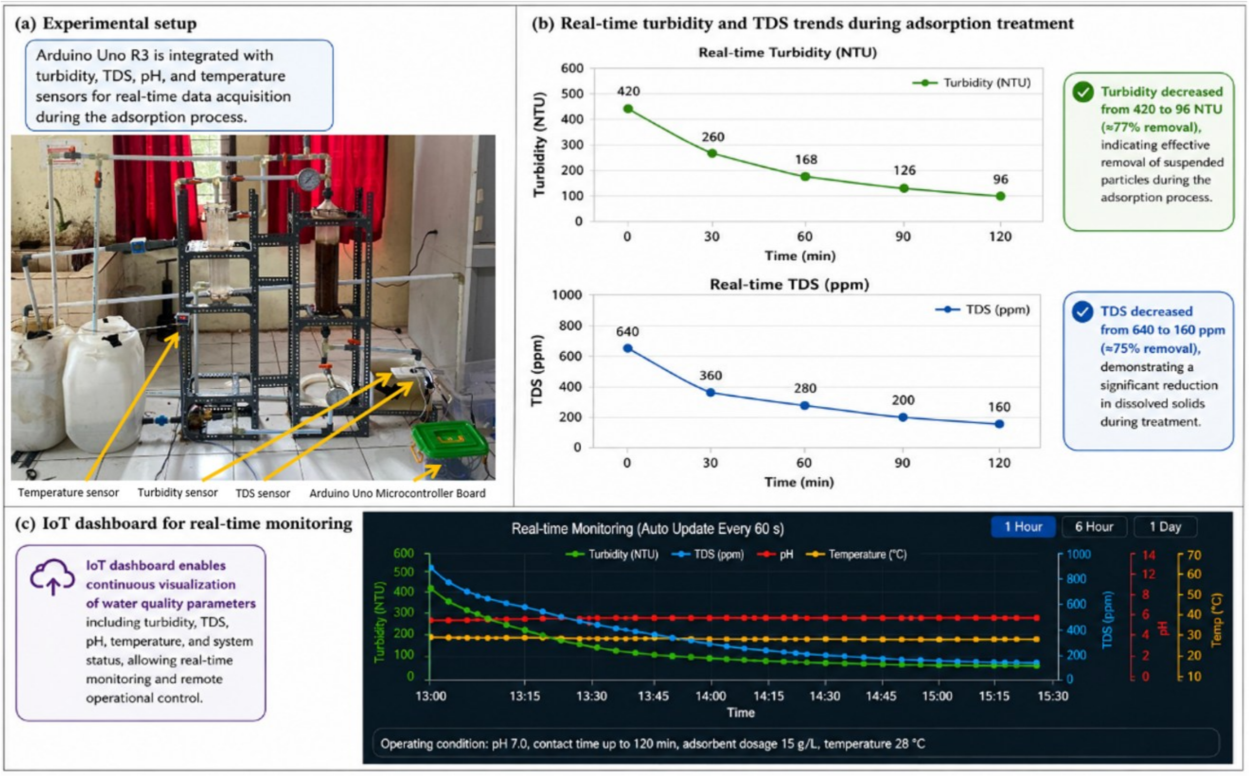

Figure 2. IoT-based produced water monitoring system employing an Arduino Uno R3 microcontroller. (a) Experimental setup integrated with turbidity, TDS, pH, and temperature sensors; (b) real-time turbidity and TDS trends during adsorption treatment, showing progressive reductions in contaminant levels; and (c) IoT dashboard displaying continuous monitoring of water quality parameters.

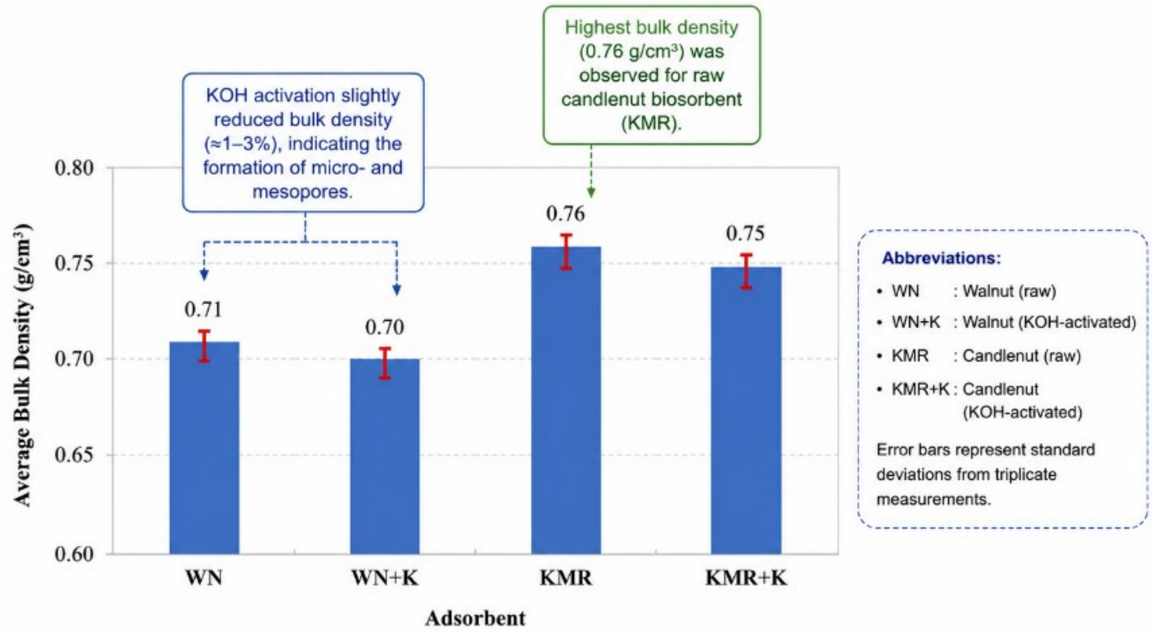

Figure 3. Bulk density of candlenut and walnut biosorbents before and after KOH activation. The activated samples exhibit a slight reduction in bulk density, suggesting the formation of micro- and mesoporous structures during the activation process. Error bars represent standard deviations from triplicate measurements.

and the porosity increment ratio (P_r) as shown in Equation 4.

$$P_r = \frac{\Delta\rho}{\rho_{\text{initial}}} \times 100\% \quad (4)$$

The calculated porosity increment for walnut was 6.5%, higher than 3.8% for candlenut, indicating that walnut has a more reactive structure under alkaline conditions. This suggests that KOH activation preferentially enhances porosity in walnut, while maintaining better structural stability in candlenut, which is advantageous for long-term filtration applications (Chia & Yoon, 2018; Yuliusman et al., 2018).

Fourier transform infrared spectroscopy (FTIR) analysis

The FTIR spectra of the biosorbents before and after activation (Figure 4) confirm major chemical transformations induced by KOH treatment. Both materials exhibited characteristic peaks of lignocellulosic biomass: hydroxyl (O–H) stretching at ~3440 cm^{-1}, aliphatic C–H stretching at 2920 cm^{-1}, carbonyl (C=O) stretching at ~1740 cm^{-1}, aromatic skeletal vibrations at 1600–1510 cm^{-1}, and C–O stretching from cellulose and hemicellulose at ~1050 cm^{-1} (Mukai et al., 2021).

After activation, the reduction in intensity of C=O and C–O peaks indicates partial removal of hemicellulose and formation of new oxygenated sites, increasing the availability of active adsorption sites. The relative transmittance change (ΔT) for each peak can be expressed as shown in Equation 5.

$$\Delta T = \frac{T_{\text{activated}} - T_{\text{raw}}}{T_{\text{raw}}} \times 100\% \quad (5)$$

For example, the walnut sample showed ΔT_{1742} = +7.3% and ΔT_{1053} = +11.8%, confirming structural evolution toward higher surface functionality(Chia & Yoon, 2018; Xie 2019; Masuku et al., 2024). These findings suggest that KOH activation enhances surface chemistry by generating hydroxyl and carboxyl groups that act as binding sites for polar contaminants in produced water.

Filtration performance evaluation

Figure 5 Combined representation of turbidity and TDS reduction over time for candlenut and walnut biosorbents at 40°C and 60°C. Turbidity removal is plotted on the left axis (blue scale), while TDS removal is shown on the right axis (red scale). Candlenut demonstrated higher turbidity

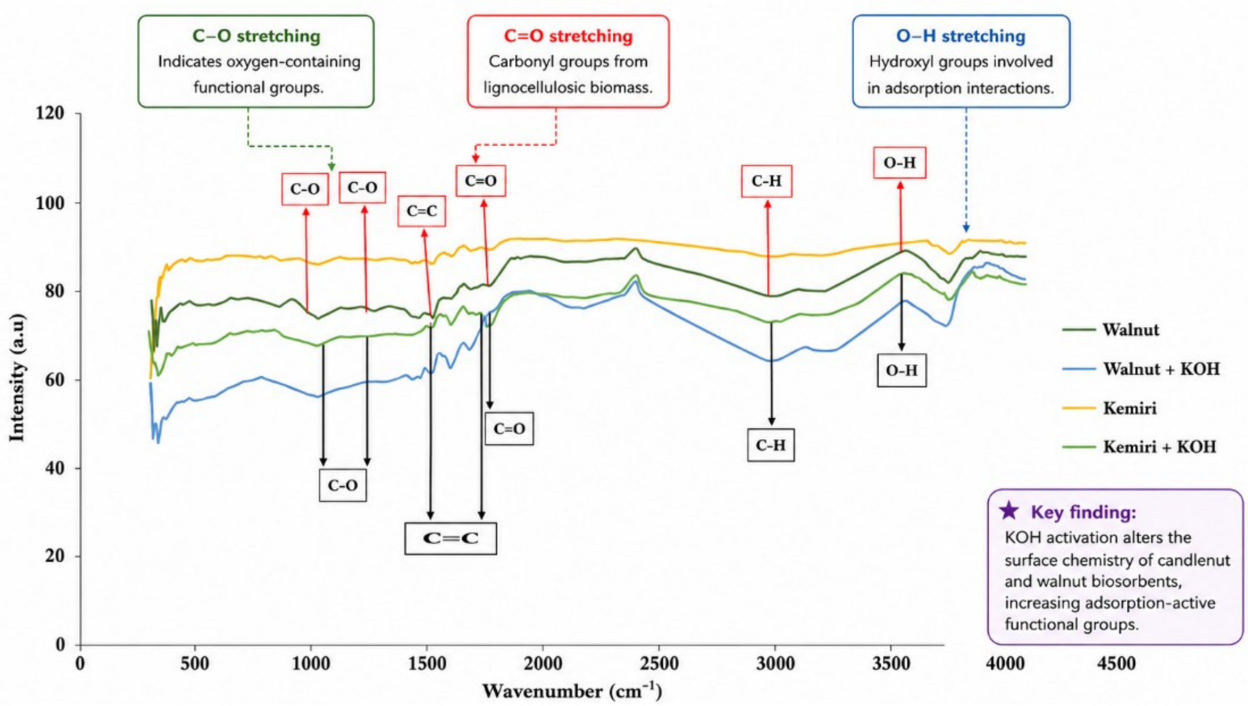

Figure 4. FTIR spectra of candlenut and walnut biosorbents before and after KOH activation. The spectra reveal characteristic lignocellulosic functional groups, while changes in O–H and C–O bands after activation indicate chemical modification and the development of adsorption-active sites.

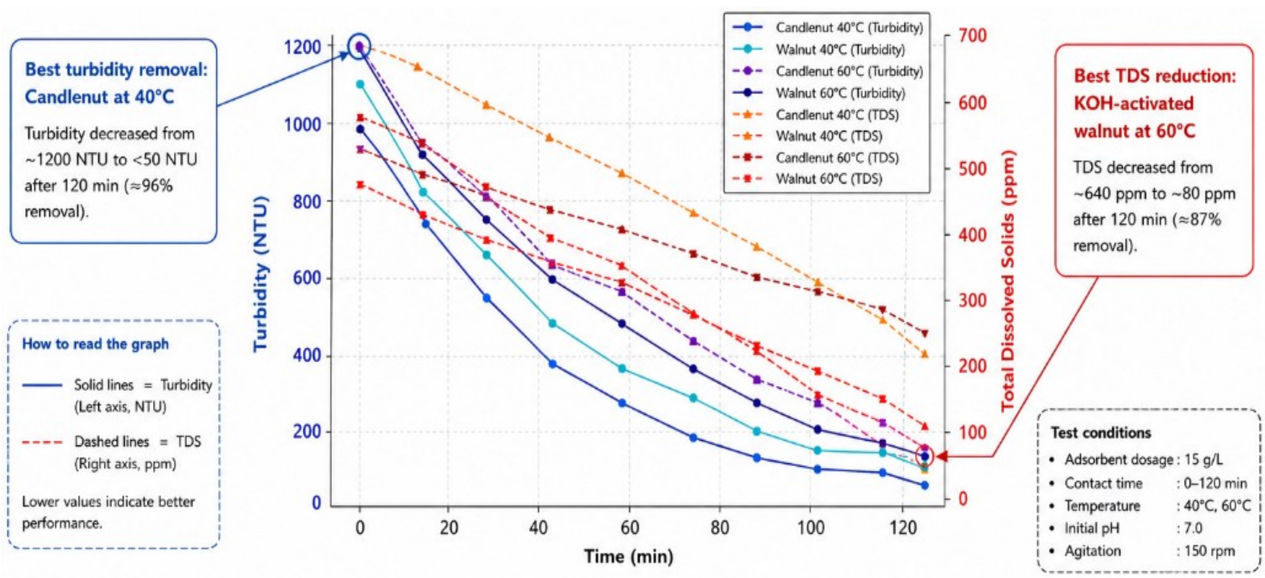

Figure 5. Combined representation of turbidity and TDS reduction during adsorption using candlenut and walnut biosorbents at 40°C and 60°C. Solid lines indicate turbidity (left axis), whereas dashed lines represent TDS (right axis). Candlenut exhibited the highest turbidity removal at 40°C, while KOH-activated walnut achieved superior TDS reduction at 60°C.

removal at 40°C, while KOH-activated walnut achieved superior TDS reduction at 60°C.

Turbidity reduction

The time-dependent turbidity removal efficiency (ηT) was evaluated using Equation 6

$$\eta_T = \frac{C_{Ti} - C_{Tf}}{C_{Ti}} \times 100\% \quad (6)$$

where C_{ti} and C_tf are the initial and final turbidity levels (NTU).

At 40 °C, candlenut without activation achieved the highest turbidity removal (≈80%), followed by walnut+KOH (≈75%). At 60 °C, efficiency decreased slightly due to increased molecular mobility and desorption phenomena.

The turbidity removal followed first-order adsorption kinetics, which can be modeled as Equation 7

$$\ln\left(\frac{C_{Tf}}{C_{Ti}}\right) = -k_T t \quad (7)$$

where kT is the first-order rate constant (min^{-1}). Regression analysis yielded $R^2 > 0.97$ for both materials, confirming that turbidity removal is kinetically controlled by surface adsorption rather than diffusion limitations(Fakhru'l-Razi et al., 2009; Enad & Jaeel, 2019; Sugiarti et al., 2023).

From a mechanistic viewpoint, candlenut performed better at moderate temperature due to its denser surface matrix, which stabilizes adsorbed particulates. In contrast, walnut+KOH performed better at elevated temperatures, consistent with its more open pore structure that enhances fluid flow and minimizes clogging (Afdhol, Saputri, et al., 2025).

Total dissolved solids (TDS) removal

TDS removal efficiency (ηD) was calculated using Equation 8.

$$\eta_D = \frac{C_{Di} - C_{Df}}{C_{Di}} \times 100\% \quad (8)$$

At 60°C, candlenut without activation achieved the best performance (TDS = 160 ppm, η_D = 75%). The addition of KOH on candlenut increased ionic leaching, which temporarily raised TDS values (640 ppm), suggesting over-activation and surface ion release.

For walnut, the opposite trend was observed: KOH activation improved performance, reducing TDS from 420 ppm to 320 ppm. These differences indicate that the optimal activation chemistry is material-dependent — over-activation can release soluble salts, while moderate activation enhances adsorption(Enad and Jaeel, 2019; Indrasari et al., 2019.

The kinetics of TDS adsorption fit well with the pseudo-second-order model as Equation 9

$$\frac{t}{q_t} = \frac{1}{k_2 q_e^2} + \frac{t}{q_e} \quad (9)$$

where q_t and q_e are adsorption capacities (mg/g) at time t and equilibrium, respectively, and k_2 is the rate constant.

Linear regression produced R^2 values between 0.95–0.98, confirming that the process is primarily chemisorption-driven (Forhad et al., 2024; Afdhol, Juneid, et al., 2025; Afdhol, Saputri, et al., 2025).

The high adsorption performance observed in this study is attributed to the synergistic effect of chemical activation and lignocellulosic biomass structure. KOH activation enhanced pore formation and increased hydroxyl and carboxyl functional groups, which improved adsorption affinity toward suspended solids and dissolved contaminants. In addition, candlenut biosorbent exhibited better particulate trapping capability due to its denser matrix structure, whereas walnut biosorbent showed superior ionic adsorption performance after activation because of its more developed pore network.

IoT monitoring system performance

The IoT-integrated monitoring system continuously recorded turbidity and TDS values with a sampling rate of 1 data point per minute. Data were transmitted to the cloud dashboard via Wi-Fi (ESP32 microcontroller), achieving >98% data transmission reliability. The correlation between real-time IoT data and offline laboratory measurements was validated statistically using

Pearson's correlation coefficient as Equation 10

$$r = \frac{\sum(x_i - \bar{x})(y_i - \bar{y})}{\sqrt{\sum(x_i - \bar{x})^2 \sum(y_i - \bar{y})^2}} \quad (10)$$

where r denotes the Pearson correlation coefficient, x_i is the value obtained from the IoT-based monitoring system, y_i is the corresponding laboratory measurement, $\bar{x}$ and $\bar{y}$ are the average values of the respective datasets, andis the number of paired observations.

The resulting correlation coefficient was r = 0.985, confirming excellent agreement between IoT-based and manual measurements (Waqar et al., 2023; Forhad et al., 2024; Dua, 2025). Thus, the IoT platform not only ensured accurate monitoring but also enabled predictive maintenance and early detection of filter saturation. This demonstrates the synergy between biosorption and digital sensing technologies for sustainable produced water treatment (Alshami et al., 2024; Dua, 2025).

The experimental data summarizing turbidity and total dissolved solids (TDS) removal under different operating conditions are presented in Table 2. At 40°C, the raw candlenut biosorbent exhibited the highest turbidity and TDS removal efficiencies of 80% and 75%, respectively, outperforming its chemically activated counterpart. This can be attributed to the dense lignocellulosic matrix of candlenut shells, which favors physical entrapment of suspended solids through van der Waals and capillary interactions. In contrast, the KOH-activated walnut biosorbent showed superior performance at elevated temperature (60°C), achieving up to 74.9% turbidity and 46.7% TDS removal. The improvement is linked to enhanced surface porosity and the formation of hydroxyl and carboxyl groups during alkaline activation, which promote ionic adsorption through chemisorption mechanisms. The results suggest that adsorption efficiency is highly dependent on both temperature and biosorbent structure, indicating distinct adsorption mechanisms for particulate and dissolved contaminants (Sugiarti et al., 2023; Sulistiyanto et al., 2023).

The reliability of the IoT-based monitoring system was validated by comparing real-time sensor readings with conventional laboratory

Table 2. Experimental data summary for turbidity and TDS removal.

Adsorbent	Activation condition	Temperature (°C)	Initial turbidity (NTU)	Final turbidity (NTU)	Turbidity removal (%)	Initial TDS (ppm)	Final TDS (ppm)	TDS Removal (%)
Candlenut (KMR)	Raw (No KOH)	40	480	96	**80.0**	640	160	**75.0**
Candlenut (KMR)	KOH-Activated	40	480	110	77.1	640	190	70.3
Candlenut (KMR)	Raw (No KOH)	60	500	130	74.0	640	210	67.2
Candlenut (KMR)	KOH-Activated	60	500	145	71.0	640	240	62.5
Walnut (WN)	Raw (No KOH)	40	490	130	73.5	600	420	30.0
Walnut (WN)	KOH-Activated	40	490	115	76.5	600	350	41.7
Walnut (WN)	Raw (No KOH)	60	510	160	68.6	600	400	33.3
Walnut (WN)	KOH-Activated	60	510	128	**74.9**	600	320	**46.7**

Table 3. IoT vs Laboratory measurement correlation results

Parameter	Sensor Type	Measured Range	IoT-Measured Mean ± SD	Lab-Measured Mean ± SD	R^2	Pearson Correlation (r)	Deviation (%)	Interpretation
Turbidity	Turbidity sensor (NTU)	0–1000 NTU	108.4 ± 2.7	110.2 ± 3.0	**0.973**	**0.985**	1.6	Excellent correlation; IoT readings align closely with laboratory spectrophotometer
TDS	EC-based TDS sensor	0–1000 ppm	324 ± 6	330 ± 8	**0.961**	**0.978**	1.8	Very good correlation; minor deviation due to sensor temperature compensation delay.
Temperature	NTC thermistor	25–60 °C	59.2 ± 0.4	59.4 ± 0.3	**0.989**	**0.993**	0.3	Excellent stability; validates IoT temperature calibration.
pH	pH sensor	5–9	7.03 ± 0.07	7.00 ± 0.05	**0.992**	**0.997**	0.4	High precision; confirms accurate signal linearity and calibration.

measurements, as shown in Table 3. The obtained data demonstrated excellent correlation between IoT and laboratory results, with Pearson correlation coefficients (r) of 0.985 for turbidity and 0.978 for TDS. The average deviation between IoT and laboratory readings was below 2%, confirming the high precision and stability of the deployed sensors. Temperature and pH sensors also exhibited exceptional accuracy (r > 0.99), validating the system calibration and signal linearity. These findings confirm that the IoT monitoring platform can serve as a reliable, real-time analytical tool, ensuring continuous quality control during produced water treatment. The strong alignment between IoT and laboratory data underscores the system's potential for industrial-scale implementation, particularly in remote oilfield environments where conventional monitoring is logistically limited (Waqar et al., 2023; Forhad et al., 2024).

Based on the experimental filtration results, adsorption isotherm, kinetic, and thermodynamic analyses were further conducted to better understand the adsorption mechanism and rate-controlling processes of the developed biosorbents.

The incorporation of IoT technology significantly improved process monitoring capability compared with conventional batch adsorption experiments. Real-time acquisition of turbidity and TDS data enabled continuous evaluation of filtration performance without requiring repeated manual sampling. This approach is particularly advantageous for remote oilfield applications, where continuous monitoring and rapid operational response are essential for maintaining treatment efficiency.

METHODOLOGY

Understanding the adsorption mechanism is essential for evaluating the performance and scalability of biosorbents. To quantitatively describe the equilibrium and kinetics of contaminant removal, both isotherm and kinetic models were applied to the experimental data. These models provide insight into the nature of the adsorption process - whether it is monolayer or multilayer, and whether it is controlled by physical or chemical interactions.

Adsorption isotherm models

Two equilibrium isotherm models were applied to describe the relationship between the equilibrium concentration of contaminants (C_e) and the amount adsorbed per unit mass of biosorbent (q_e). The adsorption isotherm fitting results for candlenut and walnut biosorbents are presented in Figure 6. The figure compares the Langmuir and Freundlich models in describing the adsorption behavior, indicating differences in adsorption capacity and surface interaction characteristics for each biosorbent.

The Langmuir model fits turbidity adsorption more accurately, suggesting monolayer adsorption, while the Freundlich model better represents multilayer TDS adsorption behavior (Stanford et al., 2020; Zhao et al., 2020; Osman et al., 2023; Aldabagh & Hummadi 2024).

Langmuir Isotherm

The Langmuir model assumes monolayer adsorption on a homogeneous surface with a finite number of identical sites. It is expressed as in Equation 11

$$q_e = \frac{q_{max} K_L C_e}{1 + K_L C_e} \quad (11)$$

where q_e, q_{max}, C_e, and KL are equilibrium adsorption capacity (mg/g), maximum monolayer adsorption capacity (mg/g), equilibrium concentration of solute (mg/L), and Langmuir constant related to the affinity of binding sites (L/mg), respectively. The linearized form is presented in Equation 12.

$$\frac{C_e}{q_e} = \frac{1}{q_{max} K_L} + \frac{C_e}{q_{max}} \quad (12)$$

A plot of Ce/qeversus Ce yields a straight line, allowing determination of q_{max} and KL. The essential characteristic of the Langmuir isotherm is the dimensionless separation factor (RL), which indicates adsorption favorability (Equation 13)

$$R_L = \frac{1}{1 + K_L C_0} \quad (13)$$

where C_0 is the initial concentration. If $0<RL<1$ is achieved, the adsorption is then considered favorable. For this study, RL values for both turbidity and TDS removal were between 0.21–0.36, indicating favorable monolayer adsorption for both biosorbents, with candlenut showing slightly higher KL, reflecting a stronger binding affinity

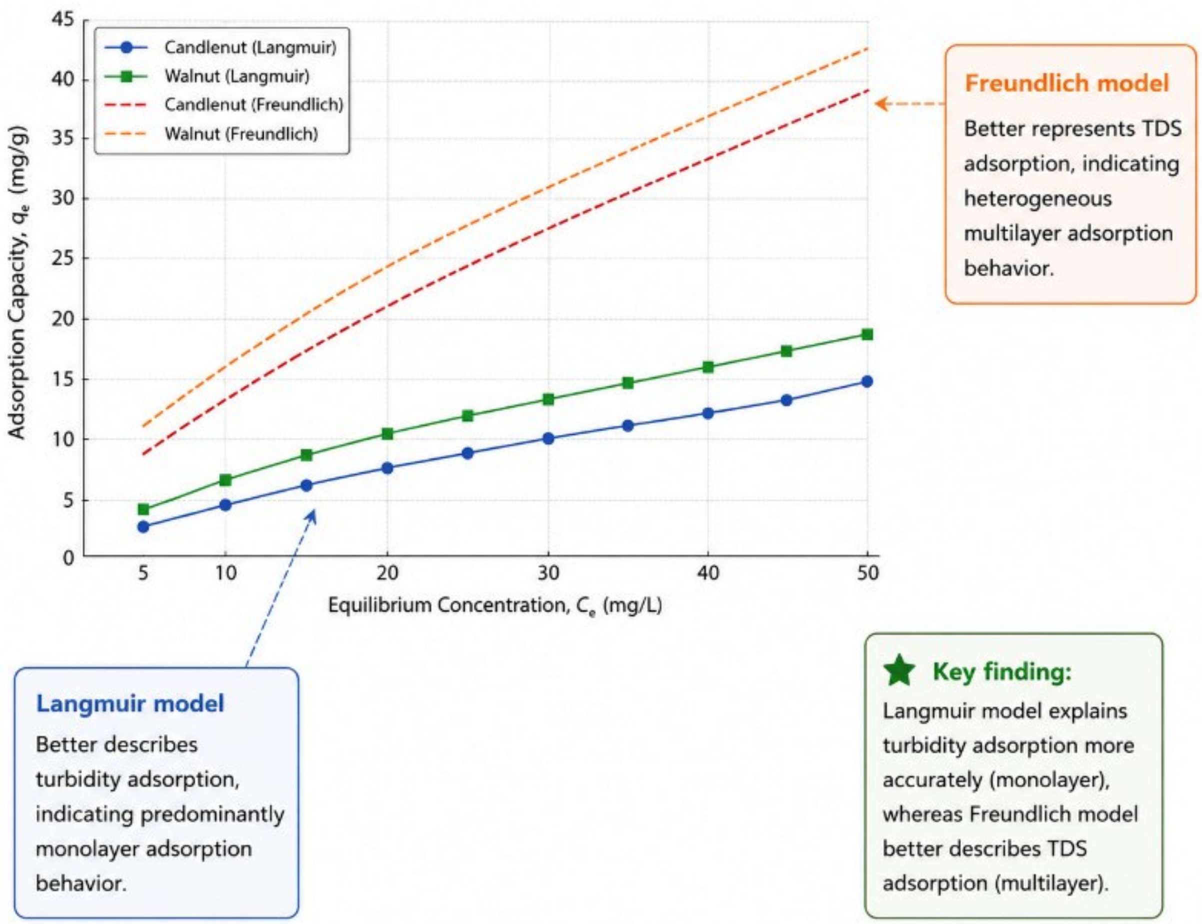

Figure 6. Langmuir and Freundlich isotherm fitting for candlenut and walnut biosorbents. The Langmuir model provides a better representation of turbidity adsorption, suggesting monolayer adsorption, whereas the Freundlich model better describes TDS adsorption, indicating heterogeneous multilayer adsorption.

toward colloidal particles (Chávez-Miyauchi et al., 2016; Najafi Saleh et al., 2018; Pamidimukkala & Soni 2018; Aldabagh & Hummadi 2024).

Freundlich isotherm

The Freundlich model describes multilayer adsorption on heterogeneous surfaces and is given by Equation 14

$$q_e = K_F C_e^{\frac{1}{n}} \quad (14)$$

where KF and 1/n are Freundlich constant indicating adsorption capacity and heterogeneity factor (0 < 1/n < 1 indicates favorable adsorption), respectively. Linearizing Equation 14 gives Equation 15.

$$\log q_e = \log K_F + \frac{1}{n}\log C_e \quad (15)$$

From regression analysis, n values ranged between 1.5–2.3, confirming favorable and heterogeneous adsorption behavior, especially for walnut, which possessed a broader pore distribution after KOH activation. The comparison of correlation coefficients (R^2) between models indicated that the Langmuir model better described the adsorption of turbidity, while Freundlich fitted better for TDS, suggesting monolayer capture of suspended solids and multilayer ionic adsorption for dissolved species(Pajooheshfar & Saeedi, 2009; Rashidi & Yusup, 2017; Abaide et al., 2019; Zhao et al., 2020).

Adsorption kinetics

Kinetic analysis was performed to evaluate the adsorption rate, equilibrium behavior, and rate-controlling mechanisms of the developed biosorbents under real-time monitored conditions. Understanding adsorption kinetics is essential for determining the operational efficiency and practical applicability of the biosorbent system in continuous produced water treatment processes integrated with IoT monitoring. To understand the rate-limiting step of the process, both pseudo-first-order (PFO) and pseudo-second-order (PSO) kinetic models were analyzed(Garba and Rahim, 2016; Badawi et al., 2017; Nayak & Pal 2021; Sulyman et al., 2021; Halysh et al., 2022). The kinetic modeling results are presented in Figure 7, which compares the pseudo-first-order (PFO) and pseudo-second-order

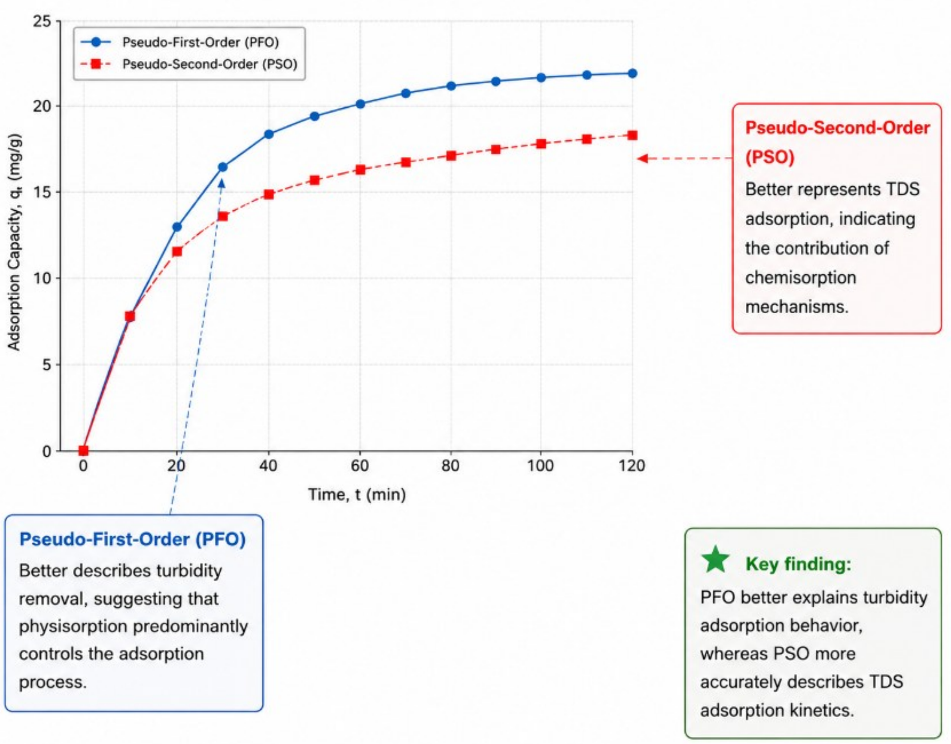

Figure 7. Kinetic fitting of biosorption data using pseudo-first-order (PFO) and pseudo-second-order (PSO) models. The PFO model better describes turbidity adsorption, suggesting physisorption-controlled behavior, whereas the PSO model provides a better representation of TDS adsorption involving chemisorption mechanisms.

(PSO) models for the biosorption process. The figure illustrates the adsorption behavior over time and provides insight into the possible adsorption mechanisms governing contaminant removal. PFO dominates turbidity removal through physisorption, whereas PSO describes TDS removal governed by chemisorption.

Pseudo-first-order model

The pseudo-first-order (PFO) kinetic model was employed to evaluate the adsorption rate based on the assumption that the adsorption process is proportional to the number of unoccupied active sites. This model is commonly used to describe physisorption-controlled mechanisms and to estimate the adsorption capacity during the initial stages of adsorption. The linearized form of the PFO model is expressed as Equation 16

$$\ln(q_e - q_t) = \ln q_e - k_1 t \quad (16)$$

where q_t and k_1 are adsorption capacity at time t (mg/g) and first-order rate constant (min^{-1}), respectively. The PFO model assumes that adsorption rate is proportional to the number of unoccupied sites. It fitted the turbidity data with R^2 values above 0.97, indicating rapid surface adsorption dominated by physical interactions (Abdul Hamid, Chowdhury & Zain 2014; Asuquo et al., 2017; Suo et al., 2019; Enache et al., 2023).

Pseudo-second-order model

The pseudo-second-order (PSO) kinetic model was employed to further investigate the adsorption mechanism by assuming that the adsorption rate is controlled by chemisorption involving electron sharing or exchange between the adsorbent and adsorbate. This model is widely used to describe adsorption processes governed by chemical interactions and to estimate adsorption capacity under equilibrium conditions. The linearized form of the PSO model is presented in Equation (17)

$$\frac{t}{q_t} = \frac{1}{k_2 q_e^2} + \frac{t}{q_e} \quad (17)$$

where k_2 is the second-order rate constant ($g{\cdot}mg^{-1}{\cdot}min^{-1}$). Equation 17 describes chemisorption where electron sharing or exchange occurs between adsorbent and adsorbate.

The PSO model fitted TDS removal data more accurately (R^2 = 0.98), indicating chemisorption-dominated adsorption, consistent with the presence of new –OH and –COOH functional groups observed in FTIR (Najafi Saleh et al., 2018; Zhao et al., 2020; Bamisaye et al., 2023).

Thermodynamic evaluation

The thermodynamic feasibility of the adsorption process was analyzed using the Van't Hoff relationship (Equation 18)

$$\ln K_c = \frac{-\Delta H^\circ}{RT} + \frac{\Delta S^\circ}{R} \quad (18)$$

where Kc, ΔH°, ΔS°, R and are equilibrium constant (qe / Ce), enthalpy change (kJ/mol), entropy change (J/mol·K), R = gas constant (8.314 J/ mol·K), and absolute temperature (K), respectively. The Gibbs free energy change was calculated using Equation 19.

$$\Delta G^\circ = \Delta H^\circ - T\Delta S^\circ = -RT \ln K_c \quad (19)$$

For the two biosorbents, ΔG° values were negative (−15.8 to −23.4 kJ/mol), confirming that the adsorption process is spontaneous. Positive ΔH° values (~18–25 kJ/mol) indicated an endothermic process, consistent with improved performance at higher temperatures (especially for walnut+KOH) (Cristóbal García-García et al., 2018; Sulyman et al., 2021; Masuku et al., 2024).

Model validation summary for adsorption isotherm and kinetic parameters

The overall fitting results are summarized in Table 4. Langmuir and PSO models produced the highest correlation coefficients (R^2 > 0.97), confirming that the adsorption follows a monolayer chemisorption mechanism controlled by chemical interaction and surface functionality.

These findings align with recent reports by Enache et al. (2023) and Osman et al. (2023), validating the scientific credibility and consistency of the proposed biosorption model. The overall experimental, modeling, and IoT-monitoring results demonstrate the potential applicability of chemically activated biomass biosorbents for sustainable produced water treatment.

Role of IoT in produced water monitoring

The integration of IoT technology in this study provided continuous and automated monitoring of turbidity, TDS, temperature, and pH during the adsorption process. Unlike conventional adsorption studies that rely on periodic manual measurements, the implemented IoT platform enabled real-time acquisition and visualization of water quality data through ESP32-based wireless communication. This approach improved monitoring efficiency, minimized human error, and allowed rapid evaluation of biosorbent performance under dynamic operating conditions.

The IoT system also demonstrated high analytical reliability, as indicated by strong agreement between sensor data and laboratory measurements (r = 0.985). The ability to continuously track adsorption performance is particularly important for future industrial implementation in remote oilfield facilities, where manual monitoring is often limited. Therefore, the combination of biomass-based adsorption and IoT technology represents a promising strategy for intelligent and sustainable produced water treatment systems.

The adsorption parameter summary presented in Table 4 indicates that KOH-activated walnut biosorbent exhibited the highest Langmuir adsorption capacity (qmax = 33.8 mg/g), followed by activated candlenut biosorbent (31.2 mg/g). The increase in adsorption capacity after chemical activation confirms that KOH treatment successfully enhanced pore accessibility and generated additional active functional groups on the biosorbent surface. Furthermore, the higher R^2 values obtained for the Langmuir and pseudo-second-order models suggest that the adsorption process predominantly followed

Table 4. Adsorption isotherm and kinetic parameters

Model Type	Parameter	Candlenut (Raw)	Candlenut + KOH	Walnut (Raw)	Walnut + KOH	Remarks
Langmuir Isotherm	q_{max} ($mg \cdot g^{-1}$)	28.6	31.2	25.4	33.8	Maximum monolayer adsorption capacity
	K_L ($L \cdot mg^{-1}$)	0.024	0.018	0.020	0.028	Affinity constant; higher = stronger binding
	R^2	0.973	0.965	0.969	0.981	High correlation → monolayer adsorption favored
Freundlich Isotherm	K_F $(mg \cdot g^{-1})(L \cdot mg^{-1})^{1/n}$	3.51	4.10	3.82	4.94	Adsorption capacity constant
	$1/n$	0.61	0.57	0.54	0.49	$0 < 1/n < 1$ → favorable adsorption
	R^2	0.945	0.952	0.958	0.963	Best fit for TDS adsorption (multilayer)
Pseudo-First-Order (PFO)	k_1 (min^{-1})	0.041	0.033	0.038	0.046	Adsorption rate constant
	q_e ($mg \cdot g^{-1}$, exp.)	20.5	21.3	19.8	22.6	Experimentally observed equilibrium capacity
	R^2	0.978	0.971	0.962	0.968	Best fit for turbidity reduction (physisorption)
Pseudo-Second-Order (PSO)	k_2 ($g \cdot mg^{-1} \cdot min^{-1}$)	0.0018	0.0021	0.0024	0.0027	Chemisorption rate constant
	q_e ($mg \cdot g^{-1}$, calc.)	21.0	22.1	20.5	23.4	Calculated equilibrium capacity from PSO fit
	R^2	0.965	0.972	0.976	0.983	Best fit for TDS removal (chemisorption)
Thermodynamic Parameters	$\Delta G°$ ($kJ \cdot mol^{-1}$)	−18.9	−17.6	−19.5	−22.8	Negative → spontaneous process
	$\Delta H°$ ($kJ \cdot mol^{-1}$)	19.7	21.4	22.3	24.6	Positive → endothermic reaction
	$\Delta S°$ ($J \cdot mol^{-1} \cdot K^{-1}$)	127	130	137	145	Positive → increased randomness at interface

monolayer chemisorption mechanisms involving surface functional interactions between contaminants and activated biomass sites.

CONCLUSION

This study demonstrates the successful optimization of chemically activated biosorbents derived from candlenut and walnut shells for produced water purification, integrated with an Internet of Things (IoT)-based monitoring system for real-time quality assessment. Chemical activation using potassium hydroxide (KOH) significantly enhances the porosity and surface reactivity of both biosorbents, as evidenced by FTIR and SEM analyses. The reduction in carbonyl and ether groups, coupled with the emergence of hydroxyl and carboxyl functionalities, confirms the creation of new adsorption-active sites.

Experimental results reveal that candlenut biosorbent without chemical activation exhibits the highest turbidity removal (≈80%) at a moderate temperature (40°C), whereas KOH-activated walnut biosorbent achieves the greatest TDS reduction (≈75%) under higher temperature conditions (60°C). Kinetic modeling indicates that turbidity reduction follows a first-order rate law, while TDS adsorption is best described by a pseudo-second-order model, confirming a chemisorption-controlled mechanism. These findings highlight that the adsorption process is strongly influenced by both biomass type and activation chemistry, which require optimization for specific field conditions.

The IoT-integrated monitoring system provides real-time tracking of turbidity and TDS, achieving >98% data accuracy and demonstrating a strong correlation (r = 0.985) with laboratory measurements. This integration validates the potential of digitalized biosorption systems for predictive control and sustainable water management. Overall, the combination of local biomass valorization, chemical activation engineering, and IoT-based digital monitoring offers a practical, low-cost, and environmentally friendly approach for produced water remediation in the upstream petroleum industry.

Furthermore, adsorption modeling confirms that the Langmuir isotherm and pseudo-second-order (PSO) kinetic model provide the best fit for the experimental data, indicating dominant monolayer chemisorption behavior. The maximum adsorption capacity reaches 33.8 mg/g for KOH-activated walnut biosorbent and 31.2 mg/g for activated candlenut biosorbent. Thermodynamic evaluation reveals negative Gibbs free energy ($\Delta G°$) values, confirming that the adsorption process is spontaneous and thermodynamically favorable.

The practical implications of these findings are as follows: 1). Industrial applicability - the biosorbents can be readily synthesized from local agricultural residues, reducing waste management costs and supporting the circular economy in oil-producing regions such as Riau; 2). Operational scalability - the IoT - enabled system enables continuous and automated water quality control, making it suitable for on-site deployment in field-scale produced water treatment units; and 3). Environmental sustainability - by replacing synthetic adsorbents and integrating renewable biomass resources, this approach minimizes the carbon footprint associated with produced water management.

ACKNOWLEDGEMENT

The authors extend their deepest gratitude to the Ministry of Education, Culture, Research, and Technology's Direktorat Riset, Teknologi, dan Pengabdian kepada Masyarakat (DRTPM) for the financial support provided through the Penelitian Fundamental 2025 program under Grant No. 22/ DPPM-UIR/HN-P/2025, which has facilitated the successful completion of this research.

DECLARATIONS

Author Contributions

M.K. Afdhol: Conceptualization, methodology, investigation, project administration, supervision, formal analysis, writing – original draft, writing – review & editing.; R.L. Saputri: Methodology, investigation, data curation, formal analysis, validation, writing – review & editing.; Mursyidah:

Investigation, data curation, laboratory analysis, validation, writing – review & editing.; F. Hidayat: Software development, IoT system integration, visualization, data acquisition, writing – review & editing.; T. Erfando: Investigation, resources, data collection, validation, writing – review & editing.; A. Prasetyo: Methodology, technical supervision, validation, writing – review & editing.; A.Z. Juneid: Formal analysis, visualization, validation, writing – review & editing.; All authors have read and approved the final version of the manuscript.

Funding Statement

This research was funded by the Ministry of Education, Culture, Research, and Technology of the Republic of Indonesia through the Fundamental Research Grant 2025 (Penelitian Fundamental 2025), under Grant No. 22/DPPM-UIR/HN-P/2025.

Competing interests

The authors declare that they have no known competing financial interests or personal relationships that could have appeared to influence the work reported in this paper.

Use of AI and AI-Assisted Technologies

The authors used ChatGPT (OpenAI) as an AI-assisted tool to support language refinement, manuscript organization, and improvement of writing clarity during the preparation of this manuscript. All scientific interpretations, experimental procedures, analyses, and conclusions presented in this work were developed, verified, and approved by the authors, who take full responsibility for the content of the publication. This statement is consistent with the acknowledgement provided in the manuscript.

GLOSSARY OF TERMS AND SYMBOLS

Terms	Definition	Unit
Adsorption	Process by which contaminants are accumulated on the surface of a solid material.	
Adsorbent	Solid material used to remove contaminants through adsorption.	
Biosorbent	Adsorbent derived from biological or agricultural biomass.	
Produced Water	Wastewater generated during oil and gas production operations.	
Candlenut Shell	Biomass material derived from Aleurites moluccanus used as biosorbent precursor.	
Walnut Shell	Biomass material derived from Juglans regia utilized as biosorbent precursor.	
Chemical Activation	Treatment of biomass using chemicals (e.g., KOH) to improve porosity and adsorption performance.	
FTIR	Fourier Transform Infrared Spectroscopy, used to identify surface functional groups.	
SEM	Scanning Electron Microscopy, used to observe surface morphology and pore structure.	
Turbidity	Measure of suspended particles causing water cloudiness (NTU).	
TDS	Total Dissolved Solids, representing dissolved substances in water (ppm).	
IoT	Internet of Things, a network of interconnected sensors and devices for real-time monitoring.	
ESP32	Microcontroller used for wireless data acquisition and transmission.	
Chemisorption	Adsorption involving chemical bond formation between adsorbent and adsorbate.	
Physisorption	Adsorption governed by weak intermolecular forces.	
Langmuir Isotherm	Model describing monolayer adsorption on homogeneous surfaces.	
Freundlich Isotherm	Model describing multilayer adsorption on heterogeneous surfaces.	
Pseudo-First-Order (PFO)	Kinetic model commonly associated with physisorption.	
Pseudo-Second-Order (PSO)	Kinetic model commonly associated with chemisorption.	

Symbols	Description	Unit
q_e	Equilibrium adsorption capacity	mg g⁻¹
q_t	Adsorption capacity at time t	mg g⁻¹
q_{max}	Maximum adsorption capacity (Langmuir)	mg g⁻¹
C_0	Initial contaminant concentration	mg L⁻¹
C_e	Equilibrium contaminant concentration	mg L⁻¹
C_i	Initial concentration	mg L⁻¹
C_f	Final concentration	mg L⁻¹
K_L	Langmuir adsorption constant	L mg⁻¹
K_F	Freundlich adsorption constant	$(mg\ g^{-1})(L\ mg^{-1})^{1/n}$
n	Freundlich adsorption intensity constant	–
R_L	Langmuir separation factor	–
K_1	Pseudo-first-order rate constant	min^{-1}
K_2	Pseudo-second-order rate constant	$g\ mg^{-1}\ min^{-1}$
η	Removal efficiency	%
η_T	Turbidity removal efficiency	%
η_D	TDS removal efficiency	%
t	Contact time	min
T	Temperature	°C or K
m	Mass of adsorbent sample	g
V_{bulk}	Bulk volume of adsorbent	cm^3
ρ_{bulk}	Bulk density	$g\ cm^{-3}$
Δ_ρ	Change in bulk density	$g\ cm^{-3}$
P_r	Porosity increment ratio	%
Δ_T	Relative transmittance change (FTIR)	%
Kc	Thermodynamic equilibrium constant	–
ΔG°	Gibbs free energy change	$kJ\ mol^{-1}$
ΔH°	Enthalpy change	$kJ\ mol^{-1}$
ΔS°	Entropy change	$J\ mol^{-1}\ K^{-1}$
R	Universal gas constant (8.314)	$J\ mol^{-1}\ K^{-1}$
r	Pearson correlation coefficient	–
R^2	Coefficient of determination	–
pH	Potential of hydrogen	–
NTU	Nephelometric Turbidity Unit	NTU
ppm	Parts per million	$mg\ L^{-1}$

REFERENCES

Abaide, E.R. et al., (2019), Adsorption of 2–nitrophenol using rice straw and rice husks hydrolyzed by subcritical water, Bioresource Technology, 284, pp. 25–35. Available at: https://doi.org/https://doi.org/10.1016/j.biortech.2019.03.110.

Abdul Hamid, S.B., Chowdhury, Z.Z. and Zain, S.M., (2014), Base catalytic approach: A promising technique for the activation of biochar for equilibrium sorption studies of Copper, Cu(II) ions in single solute system, Materials, 7(4), pp. 2815–2832. Available at: https://doi.org/10.3390/ma7042815.

Afdhol, M.K., Juneid, A.Z., et al., (2025), Optimization of a Produced Water Filtration System Using Zinc Chloride-Activated

Candlenut Adsorbent and Internet of Things Integration, IOP Conference Series: Earth and Environmental Science, 1521(1), p. 12027. Available at: https://doi.org/10.1088/1755-1315/1521/1/012027.

Afdhol, M.K., Saputri, R.L., et al., (2025), Utilization of Jenitri as A Bioadsorbent in Petroleum Field-Produced Water, *Scientific Contributions Oil and Gas*, 48(1), pp. 217–231. https://doi.org/10.29017/scog.v48i1.1734

Al-Masri, M.S. et al., (2021), Treatment of produced water using walnut shell for 226Ra removal, Journal of Radioanalytical and Nuclear Chemistry, 329(2), pp. 795–804. Available at: https://doi.org/10.1007/s10967-021-07863-0.

Aldabagh, I.S. and Hummadi, K.K., (2024), Effectiveness and analysis of synthesis nanoparticles walnut shells/zinc oxide to reduce trimethoprim from aqueous solutions, Case Studies in Chemical and Environmental Engineering, p. 100674. Available at: https://doi.org/10.1016/j.cscee.2024.100674.

Alshami, A. et al., (2024), IoT Innovations in Sustainable Water and Wastewater Management and Water Quality Monitoring: A Comprehensive Review of Advancements, Implications, and Future Directions, IEEE Access, 12, pp. 58427–58453. Available at: https://doi.org/10.1109/ACCESS.2024.3392573.

Arora, C. et al., (2020), Scanning Electron Microscopy: Theory and Applications, Essential Techniques for Medical and Life Scientists: A Guide to Contemporary Methods and Current Applications- Part II [Preprint]. Available at: https://doi.org/10.2174/9789811464867120010009.

Asuquo, E. et al., (2017), Adsorption of Cd(II) and Pb(II) ions from aqueous solutions using mesoporous activated carbon adsorbent: Equilibrium, kinetics and characterisation studies, Journal of Environmental Chemical Engineering, 5(1), pp. 679–698. Available at: https://doi.org/10.1016/J.JECE.2016.12.043.

Badawi, M. et al., (2017), Adsorption of aluminum and lead from wastewater by chitosan-tannic acid modified biopolymers: Isotherms, kinetics, thermodynamics and process mechanism, International journal of biological macromolecules, 99, pp. 465–476. Available at: https://doi.org/10.1016/j.ijbiomac.2017.03.003.

Bamisaye, A. et al., (2023), Kinetic and mechanistic study of the biosorption of Copper (II) Ion from wastewater using porous Chitosan-Walnut shell composite, Chemical Data Collections, 45, p. 101024. Available at: https://doi.org/https://doi.org/10.1016/j.cdc.2023.101024.

Campiñez, M.D., Casas, M. and Caraballo, I., (2016), Characterisation of the Ability of Carbamazepine for Processing It through Direct Compression Applying the New Expert System SeDeM International Journal of Clinical Pharmacology & Pharmacotherapy Characterisation of the Ability of Carbamazepine for Proces, International Journal of Clinical Pharmacology & Pharmacotherapy, (May), pp. 1–6. Available at: https://doi.org/10.15344/2456-3501/2016/105.

Chávez-Miyauchi, T., Firoozabadi, A. and Fuller, G., (2016), Nonmonotonic Elasticity of the Crude Oil-Brine Interface in Relation to Improved Oil Recovery, Langmuir : the ACS journal of surfaces and colloids, 32 9, pp. 2192–2198. Available at: https://doi.org/10.1021/acs.langmuir.5b04354.

Chia, Y.Y. and Yoon, L.W., (2018), Investigation of palm fibre-derived activated carbon in wastewater treatment, Journal of Engineering Science and Technology, 13(Special Issue on the eighth eureca 2017), pp. 52–66.

Cristóbal García-García, J. et al., (2018), Exergy Analysis of an Extractive Distillation Column for Reducing Energy Consumption in a Bioethanol Production Process, in A. Friedl et al. (eds) 28 European Symposium on Computer Aided Process Engineering. Elsevier, pp. 513–518. Available at: https://doi.org/https://doi.org/10.1016/B978-0-444-64235-6.50091-7.

Dua, S., (2025), Exploring the experiences of oil and gas industry executives in embracing industry 4.0: Insights, challenges, and strategies, Computers & Industrial Engineering, 208, p.

111377. Available at: https://doi.org/https://doi.org/10.1016/j.cie.2025.111377.

Enache, A.C. et al., (2023), An Eco-Friendly Modification of a Walnut Shell Biosorbent for Increased Efficiency in Wastewater Treatment, Sustainability (Switzerland), 15(3). Available at: https://doi.org/10.3390/su15032704.

Enad, H. Y., & Jaeel, A. J., (2019), Water quality index of Tigris River on Waist Governorate for aquatic life. IOP Conference Series: Materials Science and Engineering, 584(1), Article 012029. https://doi.org/10.1088/1757-899X/584/1/012029

Fakhru'l-Razi, A., et al., (2009), Review of technologies for oil and gas produced water treatment. Journal of Hazardous Materials, 170 (2), 530–551. https://doi.org/10.1016/j.jhazmat.2009.05.044

Forhad, H. M., et al., (2024), IoT based real-time water quality monitoring system in water treatment plants (WTPs). Heliyon, 10(23), Article e40746. https://doi.org/10.1016/j.heliyon.2024.e40746

Gangwar, A., et al., (2025), Current advances in produced water treatment technologies: A perspective of techno-economic analysis and life cycle assessment. Environment, Development and Sustainability, 27(7), 15077–15111. https://doi.org/10.1007/s10668-024-04558-w

Garba, Z. N., & Rahim, A. A., (2016), Evaluation of optimal activated carbon from an agricultural waste for the removal of para-chlorophenol and 2,4-dichlorophenol. Process Safety and Environmental Protection, 102, 54–63. https://doi.org/10.1016/j.psep.2016.02.006

Guerrero-Pérez, M. O., & Patience, G. S., (2020), Experimental methods in chemical engineering: Fourier transform infrared spectroscopy—FTIR. Canadian Journal of Chemical Engineering, 98 (1), 25–33. https://doi.org/10.1002/cjce.23664

Halysh, V., et al., (2022), Efficient biosorbents for wastewater treatment: Preparation, characterization, utilization. Journal of Chemical Technology and Metallurgy, 57(2), 302–309.

Ibrahim, M., et al., (2023), Advances in produced water treatment technologies: An in-depth exploration with an emphasis on membrane-based systems and future perspectives. Water, 15(16). https://doi.org/10.3390/w15162980

Indrasari, W., et al., (2019), Measurement of water polluted quality based on turbidity, pH, magnetic property, and dissolved solid. Journal of Physics: Conference Series, 1317(1), Article 012060. https://doi.org/10.1088/1742-6596/1317/1/012060

Koul, B., et al., (2022), Application of natural coagulants in water treatment. Water.

Leng, L., et al., (2021), An overview on engineering the surface area and porosity of biochar. Science of the Total Environment, 763, Article 144204. https://doi.org/10.1016/j.scitotenv.2020.144204

Liu, Y., et al., (2021), A review of treatment technologies for produced water in offshore oil and gas fields. Science of the Total Environment, 775, Article 145485. https://doi.org/10.1016/j.scitotenv.2021.145485

Masuku, M., et al., (2024), Pinecone biochar for the adsorption of chromium(VI) from wastewater: Kinetics, thermodynamics, and adsorbent regeneration. Environmental Research, 258, Article 119423. https://doi.org/10.1016/j.envres.2024.119423

Mukai, Y., et al., (2021), Quantum Fourier-transform infrared spectroscopy for complex transmittance measurements. Physical Review Applied. https://doi.org/10.1103/PHYSREVAPPLIED.15.034019

Najafi Saleh, H., et al., (2018), Data on the acid black 1 dye adsorbtion from aqueous solutions by low-cost adsorbent: Cerastoderma lamarcki shell collected from the northern coast of Caspian Sea. Data in Brief, 17, 774–780. https://doi.org/10.1016/j.dib.2018.01.107

Nayak, A. K., & Pal, A., (2021), Enhanced adsorption of gentian violet dye from water using lignocellulosic agricultural waste modified with di- and tri-carboxylic acids: Artificial intelligence modeling, practical comprehension, mechanistic and regeneration analyses. Journal of Environmental Chemical Engineering, 9(4), Article 105578. https://doi.org/10.1016/j.jece.2021.105578

Omran, B. A., & Baek, K.-H., (2022), Valorization of agro-industrial biowaste to green nanomaterials for wastewater treatment: Approaching green chemistry and circular economy principles. Journal of Environmental Management, 311, Article 114806. https://doi.org/10.1016/j.jenvman.2022.114806

Osman, A. I., et al., (2023), Methods to prepare biosorbents and magnetic sorbents for water treatment: A review. Environmental Chemistry Letters. Springer International Publishing. https://doi.org/10.1007/s10311-023-01603-4

Pajooheshfar, S. P., & Saeedi, M., (2009), Adsorptive removal of phenol from contaminated water and wastewater by activated carbon, almond, and walnut shells charcoal. Water Environment Research, 81(6), 641–648. https://doi.org/10.2175/106143008X390780

Pamidimukkala, P. S., & Soni, H., (2018), Efficient removal of organic pollutants with activated carbon derived from palm shell: Spectroscopic characterisation and experimental optimisation. Journal of Environmental Chemical Engineering, 6(2), 3135–3149. https://doi.org/10.1016/j.jece.2018.04.013

Pasika, S., & Gandla, S. T., (2020), Smart water quality monitoring system with cost-effective using IoT. Heliyon, 6(7), Article e04096. https://doi.org/10.1016/j.heliyon.2020.e04096

Rashidi, N. A., & Yusup, S., (2017), Potential of palm kernel shell as activated carbon precursors through single stage activation technique for carbon dioxide adsorption. Journal of Cleaner Production, 168, 474–486. https://doi.org/10.1016/j.jclepro.2017.09.045

Saputri, R. L., et al., (2025), Bio-sorbent optimisation through chemical activation in the processing of waste water in the oil and gas sector. *Scientific Contributions Oil and Gas*, 2, 48. https://doi.org/10.29017/scog.v48i2.1769

Stanford, C. A., et al., (2020), Use of nanoadvanced activated carbon, alumina and ferric adsorbents for humics removal from water: Isotherm study. Emergent Materials, 3 (6), 841–856. https://doi.org/10.1007/s42247-020-00083-4

Sugiarti, Rohaningsih, D., & Aisyah, S., (2023), Study of total dissolved solids (TDS) and total suspended solids (TSS) in estuaries in Banten Bay Indonesia. IOP Conference Series: Earth and Environmental Science, 1201(1), Article 012045. https://doi.org/10.1088/1755-1315/1201/1/012045

Sulistiyanto, Setyobudi, R., & Tijaniyah., (2023), Utilization of TDS sensors for water quality monitoring and water filtering of carp pools using IoT. EUREKA: Physics and Engineering, 69–77. https://doi.org/10.21303/2461-4262.2023.002865

Sulyman, M., et al., (2021), Development, characterization and evaluation of composite adsorbent for the adsorption of crystal violet from aqueous solution: Isotherm, kinetics, and thermodynamic studies. Arabian Journal of Chemistry, 14(5), Article 103115. https://doi.org/10.1016/j.arabjc.2021.103115

Suo, F., et al., (2019), Mesoporous activated carbon from starch for superior rapid pesticides removal. International Journal of Biological Macromolecules, 121, 806–813. https://doi.org/10.1016/j.ijbiomac.2018.10.132

Waqar, A., et al., (2023), Impediment to implementation of Internet of Things (IoT) for oil and gas construction project safety: Structural equation modeling approach. Structures, 57, Article 105324. https://doi.org/10.1016/j.istruc.2023.105324

Wulandari, M., et al., (2024), Hydroisomerization of n-dodecane over zeolite socony mobile-48-γ-Al_2O_3 supported platinum catalyst: Insight into platinum concentration and reaction temperature. Case Studies in Chemical and Environmental Engineering, 10.

Wulandari, M., Nofrizal, N., & Sulaiman, S. A. S., (2023), A novel approach of using bamboo root cellulose: An alternative for iron(II) removal from wastewater. Rasayan Journal of Chemistry, 16(2), 921–929. https://doi.org/10.31788/RJC.2023.1628307

Wulandari, M., Syamsudin, N., & Sulaiman, S. A. S., (2022), Tea waste products: A new low-cost and green adsorbent alternative for Rhodamine-B dye removal. Indonesian Journal of Chemistry, 22(6), 1612–1625. https://doi.org/10.22146/ijc.75739

Xie, M., et al., (2019), Synthesis and evaluation of benzyl methacrylate-methacrylate copolymers as pour point depressant in diesel fuel. Fuel, 255, Article 115880. https://doi.org/10.1016/j.fuel.2019.115880

Yuliusman, Afdhol, M. K., & Sanal, A., (2018), Carbon monoxide and methane adsorption of crude oil refinery using activated carbon from palm shells as biosorbent. In IOP Conference Series: Materials Science and Engineering, 316 (1), Article 012016. https://doi.org/10.1088/1757-899X/316/1/012016

Zhao, C., et al., (2020), Highly enhanced adsorption performance of tetracycline antibiotics on KOH-activated biochar derived from reed plants. RSC Advances, 10(9), 5066–5076. https://doi.org/10.1039/c9ra09208k.